NATIONAL ADVISORY COMMITTEE FOR AERONAUTICS

TECHNICAL NOTE 3993

BURSTING STRENGTH OF UNSTIFFENED PRESSURE

CYLINDERS WITH SLITS

By Roger W. Peters and Paul Kuhn

Langley Aeronautical Laboratory Langley Field, Va.



Washington April 1957

TECHNICAL NOTE 3993

BURSTING STRENGTH OF UNSTIFFENED PRESSURE

CYLINDERS WITH SLITS

By Roger W. Peters and Paul Kuhn

SUMMARY

Internal-pressure tests were made on aluminum-alloy unstiffened cylinders with precut slits to study the effect of slit length and curvature on the hoop stress developed at the bursting pressure. The results are predicted with good accuracy by applying a curvature correction to the method presented in NACA TN 3816 for computing the strength of flat plates with cracks. In this investigation cylinders were pressurized with air and with oil. The results indicate that the pressurizing medium has a negligible effect on the bursting pressure.

INTRODUCTION

The phenomena involved in the failure of pressurized fuselages are not well understood, and various approaches to the problem have been followed. One approach has been to investigate the static strength of flat tension specimens with fatigue cracks. This investigation has resulted in a method of strength prediction well supported by test results. (See ref. 1.)

The present paper describes an investigation of the bursting strength of 2024-T3 and 7075-T6 aluminum-alloy unstiffened cylinders which contain slits simulating cracks. It was found that the strength of these cylinders is substantially less than that of corresponding flat tension specimens. The method of strength prediction for flat specimens developed in reference 1 was extended to cover the strength of cylinders with longitudinal slits by means of an empirical curvature correction.

SYMBOLS

- b width of flat specimen, in.
- D diameter of circular hole, in.

E_n	secant modulus for nominal stress on the net section, ksi
Eu	secant modulus for ultimate stress on stress-strain curve, ksi
K _o	elastic stress-concentration factor for a circular hole in a flat sheet of finite width
Kell	elastic stress-concentration factor for an elliptical hole in a flat sheet of finite width
$K_{\mathbb{N}}$	Neuber "engineering" stress-concentration factor
K _u	stress-concentration factor for ultimate tensile strength of a flat sheet
Ku,cyl	K _u with curvature correction for cylinder
L	length of cylinder, in.
р	internal pressure, ksi
r	radius of cylinder, in.
ts	thickness of skin, in.
δ	length of slit, in.
ρ	radius of curvature, in.
ρe	effective radius of curvature, in.
$\rho_{\mathbf{u}}$	Neuber material constant for ultimate tensile strength, in.
σ	stress on gross section of flat tensile specimen, ksi
$\sigma_{ m hoop}$	nominal hoop tension stress, pr/t _S , ksi
$\sigma_{\rm u}$	ultimate tensile stress, ksi
θ	angle between slit and cylinder generatrix, deg

SPECIMENS

The specimens investigated were unstiffened circular cylinders of 2024-T3 and 7075-T6 aluminum alloy riveted to mild-steel hemispherical

domes. The domes were equipped with pipe fittings to permit connection to compressed-air or hydraulic supply lines. Two cylinder radii, 3.6 and 14.4 inches, and four nominal skin thicknesses, 0.006, 0.012, 0.016, and 0.025 inch, were the primary variables investigated. The configurations are listed in table I, and a typical cylinder is shown in figure 1.

Each cylinder had a slit, similar to that shown in figure 2, made by drilling a 1/32-inch-diameter hole in the flat sheet material and filing in opposite directions therefrom with a thin needle file. The width of the slits was about 0.008 inch and the length varied from 0.24 to 7.97 inches. The ends of the slits generally were roughly square. In flat sheet material for three cylinders a No. 80 (0.0135-inch) hole was drilled at each end of the slit (stop-drilling). Slits were cut at angles of 0°, 45°, 60°, and 90° with the longitudinal axis of the cylinder. The length of most of the 3.6-inch-radius cylinders was 20 inches but those cylinders with slit lengths of approximately 8 inches were 40 inches long. Most of the 14.4-inch-radius cylinders were 74.5 inches long but a few were 60 inches long.

The cylinders were fabricated with the sheet grain parallel to the longitudinal axis of the cylinder, except for three cylinders fabricated with the sheet grain running circumferentially to determine whether there would be any variation in the results due to sheet orientation. The cylinders with 3.6-inch radius and skins 0.006, 0.012, and 0.016 inch thick were wrapped and riveted to the domes. Those with skins 0.025 inch thick were rolled to the 3.6-inch radius before riveting to the domes. All the 14.4-inch-radius cylinders were rolled before riveting. The skin seams were made with two rows of 3/32-inch-diameter rivets spaced 1/2 inch apart. In addition, the seams were bonded with an adhesive to minimize the possibility of seam failure.

PROCEDURE

In order to prevent injury to personnel the air-pressurized 3.6-and 14.4-inch-radius cylinders were tested in steel shells of 8.0- and 30.0-inch inside diameter, respectively, as shown in figure 3. The shells were vented by large holes in the end plates and by an observation hole in the shell wall. The cylinders were inserted in the steel shells so that the slit was adjacent to the observation hole.

The procedure was to increase gradually the internal pressure until the test cylinder burst. Internal pressure was measured by a strain-gage pressure cell and recorded autographically. In most tests the time to achieve maximum pressure was between 30 and 60 seconds; the shortest time was 3 seconds and the longest time was 4 minutes. All cylinders except

four were pressurized with air. These four were pressurized with oil to determine whether or not the pressurizing medium had any effect on the pressure required to cause failure.

4

METHOD OF COMPUTATION

A method for computing the bursting strength of an unstiffened cylinder with a longitudinal slit was obtained by applying a curvature correction to the method of reference 1 for calculating the static strength of a flat tension specimen containing a crack or slit. This procedure is described in the appendix.

RESULTS AND DISCUSSION

The main results are shown in the last column of table I and in figures 4 and 5. The two top curves in each of the two figures are computed curves for flat tensile specimens $(r = \infty)$ with widths equal to the lengths of the cylinders used in the tests. The drop in nominal stress with increasing length of slit in the flat specimens is due to the combination of two factors: increase in severity of stress concentration, and decrease in the ratio of net section to gross section.

The computed curves for the cylindrical specimens are in very good agreement with the test results. (See figs. 4 and 5.) These curves and test points show that curvature introduces a substantial drop of strength below the strength computed for corresponding flat specimens $(r = \infty)$. This effect of curvature may be regarded as the most significant result of the investigation.

In figure 4 the results for cylinders with $r/t_{\rm S}$ values of 600, 300, 240, and 144 fall close to the single computed curve. Similarly, in figure 5, results for $r/t_{\rm S}$ values of 225 and 144 fall on one curve. Thus, $r/t_{\rm S}$ is not the parameter which governs the curvature correction to the stress-concentration factor. (The parameter $r/t_{\rm S}$ is, of course, a primary one in the sense that it governs the relation between internal pressure and nominal hoop tension.)

Figure 4 includes four test points for cylinders in which oil instead of air was used as the pressurizing medium. The results indicate no significant difference in bursting pressure due to the difference in pressurizing medium.

NACA IN 3993

In order to afford a direct comparison between the two materials (2024-T3 and 7075-T6), figure 6 shows test points and computed curves for comparable test series. The strength of the 7075-T6 aluminum-alloy cylinders is lower (in spite of higher material strength) because of the nature of the stress-strain curve (higher ratio of yield strength to ultimate strength) in this material, which results in higher values of $K_{\rm N}$. (See appendix.)

Figure 7 shows the effect of slit orientation on the failure of 2024-T3 aluminum-alloy cylinders with a radius of 3.6 inches. The nominal hoop stress at failure for a given slit length increases rapidly as the angle between the slit and the cylinder generatrix increases.

Figure 8 shows the effect of terminating the slits with a drilled hole having a diameter greater than the slit width (stop-drilling). The experimental gain in strength over the configurations with slit ends as filed (roughly square) ranges from 16 to 22 percent. Computations were also made for the stop-drilled configuration. The method described in the appendix was used except that the actual drill radius ρ was used instead of the effective radius ρ_e , and consequently equation (2a) was used instead of (2b). These computations showed strength gains of only 2 to 6 percent; the discrepancy between calculated and experimental gains gives some indication of the accuracy limitations of the method of computation, at least for the case of stop-drilled slits.

Although it was shown in figure 4 that cylinders pressurized with air failed at approximately the same hoop tensile stress as those pressurized with oil, the destructiveness of the failure of air-pressurized cylinders was much greater. Figure 9 shows the results of air and oil pressurization of identical cylinders that originally had 0.96-inch slits. The cylinder tested with air is split open from end dome to end dome, and the sheet is torn away from the end domes for a considerable distance around the perimeter. In the cylinder tested with oil, the fracture consists simply in an extension of the original slit on each end. This difference in destructiveness between air and oil tests has been noted by other investigators.

CONCLUSIONS

Bursting-strength tests were conducted on 58 unstiffened cylinders of 2024-T3 and 7075-T6 aluminum alloy with slits representing fatigue cracks. The test data and the analysis presented warrant the following conclusions:

1. The bursting strength (nominal hoop stress at failure) is substantially reduced by increasing the slit length and increasing the

NACA IN 3993

curvature. The effect of slit length is in line with the theory of stress concentration, but the strong effect of curvature is not explained by known theory.

- 2. The bursting strength of cylinders constructed of 7075-T6 aluminum alloy is lower than that of 2024-T3 aluminum-alloy cylinders despite the higher ultimate tensile strength of 7075-T6 aluminum alloy. This result is in agreement with predictions made by the method of NACA TN 3816 for computing the static strength of flat specimens with cracks or slits.
- 3. The bursting strength of cylinders pressurized by oil appears to be the same as the bursting strength of cylinders pressurized by air.
- 4. The bursting strength of unstiffened cylinders of 2024-T3 and 7075-T6 aluminum alloy with longitudinal slits can be predicted by applying an empirical curvature correction to the method of NACA TN 3816.

Langley Aeronautical Laboratory,
National Advisory Committee for Aeronautics,
Langley Field, Va., January 25, 1957.

APPENDIX

METHOD OF COMPUTING THE BURSTING STRENGTH OF

A CYLINDER WITH A LONGITUDINAL CRACK

Static Strength of a Flat Tension Specimen With a Crack

A method for calculating the static strength of flat tension specimens with notches, slits, or cracks has been developed previously (ref. 1). The method is based on the assumption that failure will take place when the peak stress at the root of the notch becomes equal to the tensile strength $\sigma_{\rm u}$ of the material. This peak stress is computed as the product of the average stress on the net section and a stress-concentration factor $K_{\rm u}$. The procedure for calculating the factor $K_{\rm u}$ for a centrally located crack or fine slit is reproduced here in order to make this paper self-contained.

For an elliptical hole of length δ in a flat sheet of finite width, the theoretical factor of stress concentration may be calculated by the equation

$$K_{ell} = 1 + (K_0 - 1)\sqrt{\frac{\delta}{2\rho}}$$
 (1)

where K_0 is the theoretical factor for a circular hole (see fig. 10) with a diameter D equal to the length δ of the ellipse and ρ is the tip radius of the ellipse.

For a crack or a fine slit, the theoretical factor is calculated by the same formula; the tip radius ρ is indefinite and unknown for such configurations and an effective value ρ_e is used, which is taken as 0.0036 inch for 2024-T3 and 7075-T6 aluminum alloys.

In order to allow for size effect, caused by the granular structure of the material, the theoretical factor is converted into an "engineering" stress-concentration factor, called Neuber factor, by use of the equation

$$K_{\rm N} = 1 + \frac{K_{\rm ell} - 1}{1 + \sqrt{\frac{\rho_{\rm u}}{\rho_{\rm e}}}}$$
 (2a)

where $\rho_{\rm u}$ is the specific value of the Neuber material constant applicable to ultimate strength. For the two aluminum alloys considered here $\rho_{\rm u}$ = $\rho_{\rm e}$, and the equation simplifies to

$$K_{\rm N} = 1 + \frac{1}{2}(K_{\rm ell} - 1)$$
 (2b)

The Neuber factor is converted into the final factor $K_{\rm u}$ by applying a plasticity correction:

$$K_u = 1 + (K_N - 1) \frac{E_u}{E_n}$$
 (3)

where E_u is the secant modulus pertaining to the stress σ_u , and E_n is the secant modulus pertaining to the average stress over the net section at failure. Figure 11 gives K_u as a function of K_N for the two aluminum alloys to eliminate the trial-and-error solution of equation (3).

Bursting Strength of a Cylinder With a Crack

The configuration considered here is a closed cylinder under internal pressure, with a longitudinal crack or slit located half-way between the ends of the cylinder. The cylinder is assumed to be reasonably long, so that the secondary stresses at the juncture between end dome and cylinder do not influence the stresses at the end of the crack.

If the cracked cylinder (without end domes) is considered unwrapped into a flat specimen so that the cylinder length L is equal to the flat-specimen width b, a factor $K_{\rm u}$ can be calculated by the method given in the preceding section. This factor defines the strength of the flat specimen under a tensile load in the direction of the hoop tension. In the curved (cylindrical) configuration, however, the tensile load causing failure is much less than in the flat configuration; in other words, the stress-concentration factor is higher. Empirically, it has been found that the factor for the cylinder $K_{\rm u,cyl}$ can be computed from the factor for the corresponding flat tension specimen by means of the relation

$$K_{u,cyl} = K_{u} \left[1 + 4.6 \left(\frac{\delta}{r} \right) \right]$$
 (4)

The nominal stress system at the location of the crack is biaxial: there is a hoop tension σ_{hoop} and a longitudinal tension equal to $\frac{1}{2}\sigma_{\text{hoop}}$. At the end of the crack, the hoop tension is greatly magnified by the stress-concentration action of the crack. At the same point, the longitudinal tension in the sheet creates a compressive stress numerically equal to $\frac{1}{2}\sigma_{\text{hoop}}$. The curvature correction expressed by relation (4), by virtue of its empirical derivation, includes automatically an allowance for the existence of the negative stress component set up by the longitudinal stress.

The effect of additional longitudinal stresses in the cylinder caused by loads other than the internal pressure can be neglected in most cases. If the additional stress is tensile, then the stress component at the critical point is negative; thus, to neglect it is a conservative attitude. If the additional stress is compressive, then the stress component set up by it at the critical point is tensile and should be considered in principle. However, the stress component is numerically equal to the longitudinal stress (stress-concentration factor of unity) and is thus small compared with the magnified or peak hoop stress unless the crack is very short. (For the longest cracks in the test cylinders, the compressive stress component was only about 2 percent of the peak hoop stress.)

The method of computing the bursting strength has been applied to cylinders of 2024-T3 and 7075-T6 aluminum alloy with very satisfactory results. In particular, it may be noted that the curvature correction given by relation (4) applies equally well to both materials. However, the physical nature of the curvature correction is obscure at present; consequently, great caution should be used in applying relation (4) to other structural materials, particularly in view of the fact that it appears to be definitely inapplicable to a very brittle material, namely, glass.

Bursting Strength of Glass

Bursting tests on glass tubes and bulbs were made by Griffith (ref. 2). If the glass is assumed to be perfectly brittle, that is, elastic up to fracture, and if it is assumed that the relation $\rho_{\rm U} = \rho_{\rm e}$ is applicable to glass, then, from equations (3) and (2b),

$$K_{u} = K_{N} = 1 + \frac{1}{2}(K_{ell} - 1)$$
 (5)

NACA IN 3993

The length of the tubes was not specified in reference 2, and the solution for an elliptical hole in a sphere is not known. It was assumed, therefore, that $K_{\rm O}$ had the limiting value of 3; then, from equations (1) and (5),

$$K_{u} = 1 + \sqrt{\frac{\delta}{2\rho_{e}}} \tag{6}$$

- A 10

Table II shows values of K1 calculated from equation (6), nominal hoop tensions calculated by means of Ku, and the ratios of calculated to experimental strength. The constant $\rho_e = 0.97 \times 10^{-4}$ inch was evaluated from the tests; thus, the fact that the ratio of calculated to experimental strength has an average value very close to unity has no significance. The significant observation is that this ratio for the bulb tests deviates from unity by about 4 percent at most, despite the fact that the ratio δ/r varies from 0.2 to about 0.9. If a curvature correction of the type indicated by relation (4) were applicable to glass, the numerical constant would be at most about 1/100 of the value applicable to the aluminum alloys. Inspection of the data on the glass tubes in table II gives a similar indication, although the conclusion is weaker here because the ratio δ/r covers a much smaller range. For practical purposes, the curvature correction appears to be negligible (that is, equal to unity) for glass, a radical difference from the result for aluminum alloys. This difference indicates that the curvature correction given by relation (4) is of limited scope and should not be applied to other materials without check tests for verification.

REFERENCES

- 1. McEvily, Arthur J., Jr., Illg, Walter, and Hardrath, Herbert F.: Static Strength of Aluminum-Alloy Specimens Containing Fatigue Cracks. NACA TN 3816, 1956.
- 2. Griffith, A. A.: The Phenomena of Rupture and Flow in Solids. Phil. Trans. Roy. Soc. (London), ser. A, vol. 221, Oct. 21, 1920, pp. 163-198.
- 3. Howland, R. C. J.: On the Stresses in the Neighbourhood of a Circular Hole in a Strip Under Tension. Phil. Trans. Roy. Soc. (London), ser. A, vol. 229, no. 671, Jan. 6, 1930, pp. 49-86.

TABLE I

DIMENSIONS AND TEST CONDITIONS FOR ALUMINUM-ALLOY UNSTIFFENED PRESSURIZED CYLINDERS

Cylinder	Radius, r, in.	Skin thickness, ts, in.	Alloy	Slit length, 8, in.	Slit orientation, 0, deg	Cylinder length, L, in.	Nominal hoop tension stress at max. pressure, choop, ksi
a ₂ a ₄ 5	3.6 3.6 3.6 3.6 3.6	.012 .012 .012 .012	2024-T3 2024-T3 2024-T3 2024-T3 2024-T3	0.24 .24 .50 .50	0 0 0	20 20 20 20 20	40.2 41.4 -30.6 26.4 19.9
a6 a7 8 9	3.6 3.6 3.6 3.6	.012 .012 .012 .012	2024-T3 2024-T3 2024-T3 2024-T3 2024-T3	.96 .96 1.87 3.82 7.69	0 0 0	20 40 20 20 20 40	20.4 21.0 10.7 4.9 2.6
11 12 13	3.6 3.6 3.6	.015 .015	2024-T3 2024-T3 2024-T3	.62 1.20 2.40	0 0 0	20 20 20	29.3 17.2 8.7
14 15 16	3.6 3.6 3.6	.025 .025 .025	2024-T3 2024-T3 2024-T3	1.03 2.00 5.63	0 0	20 20 20	21.9 10.4 3.4
17 18 19 20	3.6 3.6 3.6 3.6	.006 .006 .006	2024-T3 2024-T3 2024-T3 2024-T3	.24 .47 .96 1.96	0 0	20 20 20 20	44.4 27.3 20.7 10.2
21 22 23	3.6 3.6 3.6	.016 .016 .016	7075-16 7075-16 7075-16	.66 1.29 2.56	0 0	20 20 20	19.4 11.7 5.5
24 25 26	3.6 3.6 3.6	.025 .025 .025	7075-16 7075-16 7075-16	1.00 2.02 4.00	0 0	20 20 20	16.6 8.4 3.7
b ₂₇ b ₂₈ b ₂₉	3.6 3.6 3.6	.012 .012 .012	2024-T3 2024-T3 2024-T3	.98 1.98 4.02	0 0	20 20 20	22.9 12.8 5.7
c ₃₀ c ₃₁ c ₃₂	3.6 3.6 3.6	.012 .012 .012	2024-T3 2024-T3 2024-T3	.96 1.91 3.83	0 0	20 20 20	22.8 10.2 5.4
33 34 35	3.6 3.6 3.6	.012	2024-T3 2024-T3 2024-T3	.47 .95 7.70	30 30 30	20 20 40	36.8 22.6 2.6
36 37 38 39 40	3.6 3.6 3.6 3.6 3.6	.012 .012 .012 .012	2024-T3 2024-T3 2024-T3 2024-T3 2024-T3	.49 .97 1.93 3.84 7.75	45 45 45 45 45	20 20 20 20 40	40.0 28.0 17.6 8.0 2.2
41 42 43 44	3.6 3.6 3.6 3.6	.012 .012 .012	2024-T3 2024-T3 2024-T3 2024-T3	.45 .98 1.95 5.00	60 60 60 60	20 20 20 20	42.9 34.5 24.6 7.8
45 46 47 48 49	3.6 3.6 3.6 3.6	.012 .012 .012 .012	2024-T3 2024-T3 2024-T3 2024-T3 2024-T3	.48 .95 1.92 3.84 7.97	90 90 90 90	20 20 20 20 40	58.2 55.2 48.9 34.2 2.2
50 51 52 53 54	14.4 14.4 14.4 14.4 14.4	.015 .015 .015 .015 .015	2024-T3 2024-T3 2024-T3 2024-T3 2024-T3	.63 1.28 2.55 5.10 7.70	0 0 0 0 0	74.5 74.5 74.5 74.5 74.5	41.3 29.8 20.4 11.3 8.2
55 56 57 58	14.4 14.4 14.4 14.4	.016 .016 .017	7075-116 7075-116 7075-116 7075-116	.62 1.30 2.58 5.16	0 0	74.5 74.5 60 60	37.2 24.9 13.6 8.5

^aTested with oil pressurization.

 $^{b}\text{Ends}$ of cracks rounded (stop-drilled, ρ = 0.0068 in.).

 $^{\mathrm{c}}$ Sheet grain running circumferentially.

TABLE II

ANALYSIS OF TESTS OF REFERENCE 2 ON GLASS BULBS AND TUBES $\left[\sigma_{\text{u}} = 24.9 \text{ ksi; } \rho_{\text{e}} = 0.97 \times 10^{-4} \text{ inch} \right]$

No.	δ	Ku	Thoop, calc., ksi	choop, exp., ksi	Ratio of calc. to exp.	δ/r				
Bulbs										
1	0.15	28.8	0.865	0.864	1.001	0.201				
2	.27	38.4	.649	.623	1.041	• 353				
3	. 54	53.7	.463	.482	.961	.675				
4	.89	68.7	.362	. 366	.990	.890				
Tubes										
1	0.125	36.9	0.675	0.678	0.998	0.725				
2	.16	41.6	.598	. 590	1.012	.902				
3	.19	45.2	.550	.526	1.044	1.027				
4	.14	38.9	.640	.655	•977	.919				
5	.13	37.6	.662	.674	.982	.840				
6	.15	40.2	.620	.616	1.006	.985				

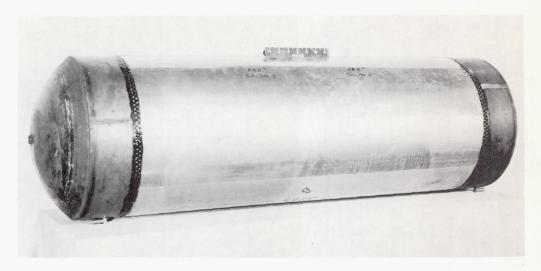


Figure 1.- Unstiffened cylinder with 14.4-inch radius.

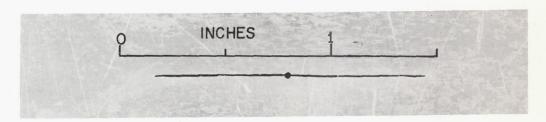
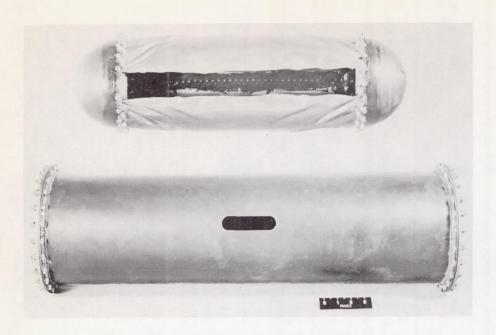
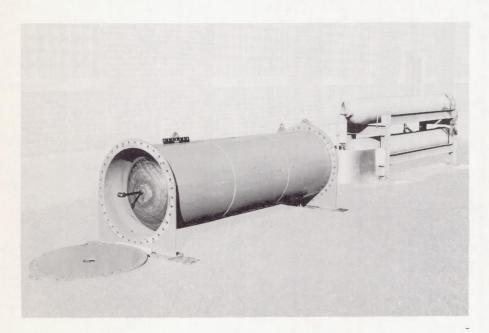


Figure 2.- Typical slit. L-57-157



(a) Cylinder with 3.6-inch radius and shell.



L-57-158

(b) Cylinder with 14.4-inch radius installed in shell.

Figure 3. - Steel shells in which unstiffened cylinders were tested.

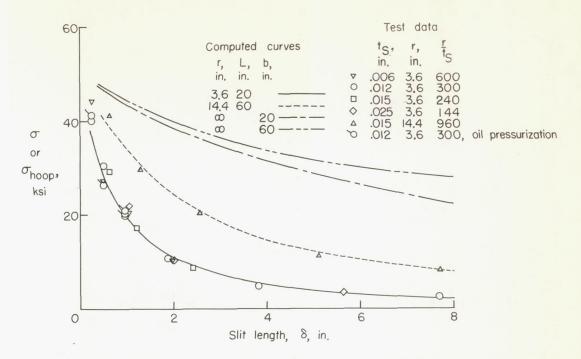


Figure 4.- Variation of hoop stress with slit length for 2024-T3 aluminumalloy unstiffened cylinders.

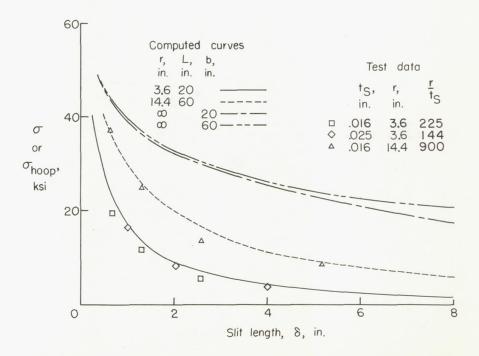


Figure 5.- Variation of hoop stress with slit length for 7075-T6 aluminumalloy unstiffened cylinders.

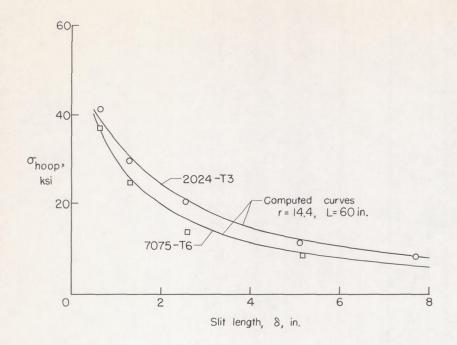


Figure 6.- Comparison of 2024-T3 with 7075-T6 aluminum-alloy unstiffened cylinders with 14.4-inch radius.

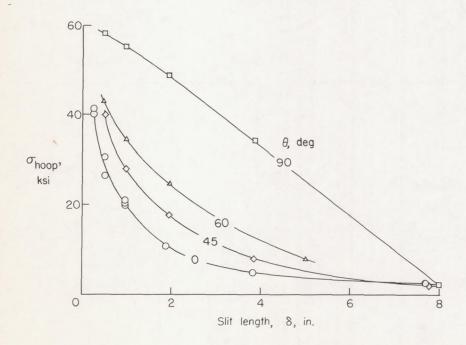


Figure 7.- Effect of slit orientation on relation between hoop stress and slit length for 2024-T3 cylinders with 3.6-inch radius and $t_S=0.012$ inch. All curves are experimental.

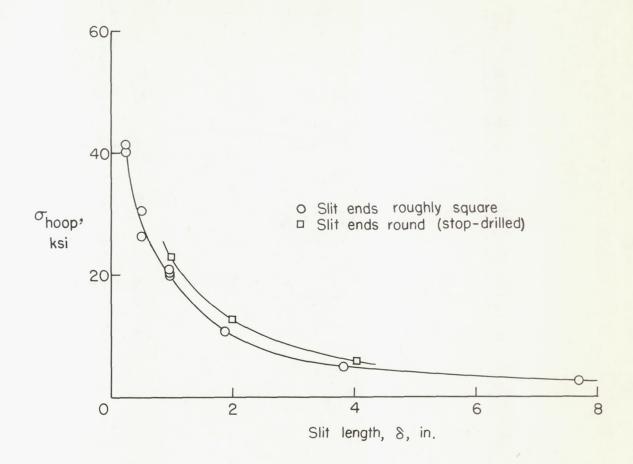
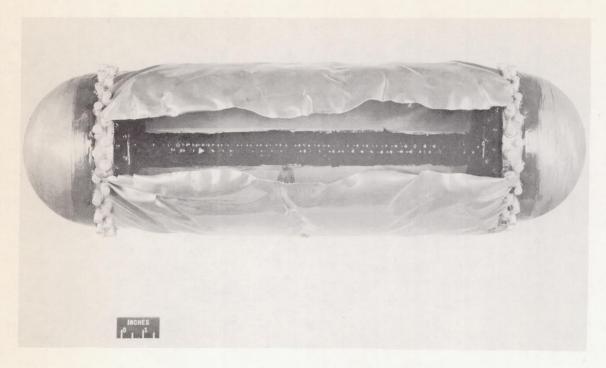
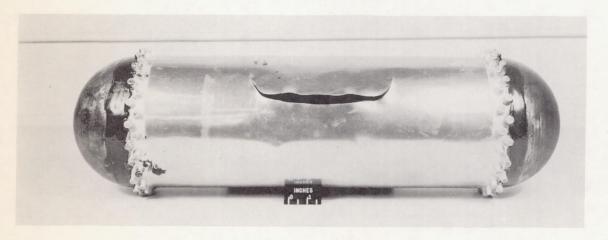


Figure 8.- Effect of rounding slit ends of 2024-T3 cylinders with 3.6-inch radius and $t_S=0.012$ inch. Both curves are experimental.



(a) Air pressurization.



(b) Oil pressurization.

L-57-159

Figure 9.- Comparison of failures of cylinders with $\delta = 0.96$ pressurized with air and oil.

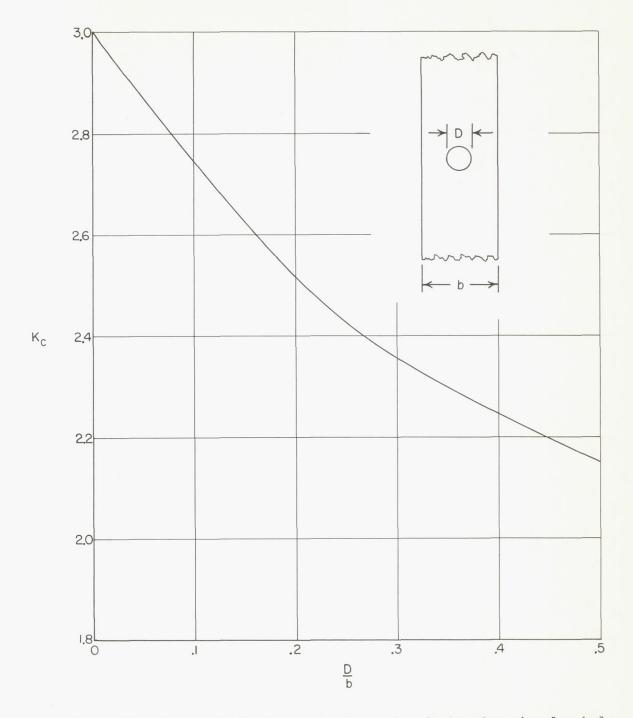


Figure 10.- Theoretical stress-concentration factor for circular hole in flat sheet of finite width (ref. 3).

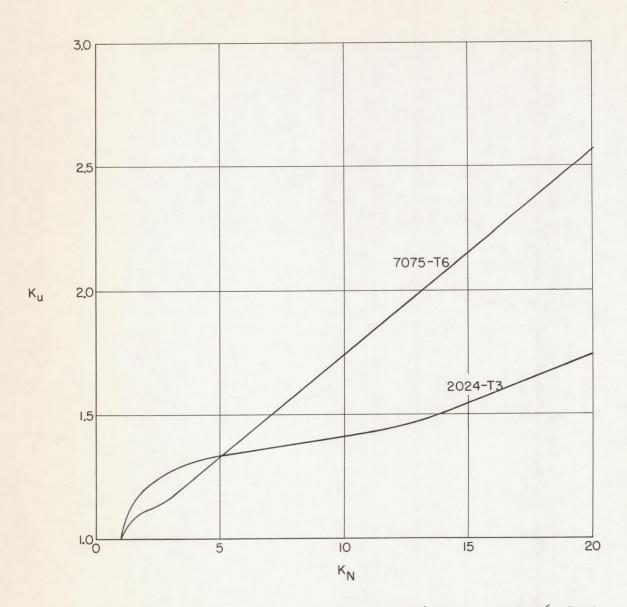


Figure 11.- Variation of $K_{\rm U}$ with $K_{\rm N}$ for 2024-T3 and 7075-T6 aluminum alloys.